Nanotubes With Well-Defined Structure: Single- and Double-Walled Imogolites

ARTICLE *in* THE JOURNAL OF PHYSICAL CHEMISTRY C · MARCH 2014

Impact Factor: 4.77 · DOI: 10.1021/jp411086f

THE JOURNAL OF PHYSICAL CHEMISTRY C

Article

pubs.acs.org/JPCC

Nanotubes With Well-Defined Structure: Single- and Double-Walled Imogolites

Maicon P. Lourenço,[†] Luciana Guimarães,[‡] Maurício Chagas da Silva,[†] Claudio de Oliveira,[‡] Thomas Heine,[§] and Hélio A. Duarte*[,†]

[†]Department of Chemistry, Instituto de Ciências Exatas, Universidade Federal de Minas Gerais, 31270-901 Belo Horizonte, Minas Gerais, Brazil

[‡]Department of Natural Science, Universidade Federal de São João Del Rei, 36301-160, São João Del Rei, Minas Gerais, Brazil

[§]School of Engineering and Science, Jacobs University Bremen, Campus Ring 1, 28759 Bremen, Germany

Supporting Information

ABSTRACT: We have investigated the structure and electronic structure of single- and double-walled imogolite nanotubes with Ge and Si as group IV element. While it is known from experiment, and in the case of single-walled tubes confirmed by theory, imogolite nanotubes are monodisperse in diameter. We show that imogolite tubes are also showing a preferred chirality (zigzag), resulting from the hydrogen-bond network on the tube surfaces, and that there is an exceptionally stable form of intertube interaction that supports the formation of monodisperse double-walled imogolite nanotubes. The strongest stabilization of double-walled tubes has been found for tube indexes with nine units of difference around the circumference, and the minimum structure is found for the (12,0)@(21,0) tube in the case of germanium imogolite and (9,0)@(18,0) for imogolite. The electronic structure is only slightly affected by these geometric factors, as are the mechanical properties, which show Young moduli of 320−370 GPa, thus being in the same range as other clay mineral nanotubes.

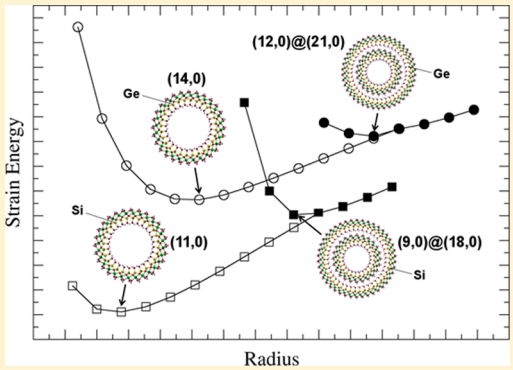

INTRODUCTION

The control of the structural properties of nanotubes (NTs) with well-defined chirality, radii, and length is of overwhelming interest for technological applications in the field of electronics, environmental sciences, biology, and engineering. In this context, clay mineral NTs of the imogolite family are exceptional, as they show truly monodisperse character with well-defined diameter, chirality, and relatively homogeneous length distribution.[1−4]

Imogolite is an aggregation of single-walled aluminosilicate NTs that are found as minerals in volcanic soils[5] and that can be easily synthesized.[6] The tube wall is composed of a gibbsite-like sheet ($Al(OH)_3$) at the outer surface, and with ((SiO_3)-OH) groups at the inner surface, giving a composition of $(HO)_3Al_2O_3SiOH$. The lattice mismatch of the orthosilicate layer causes the shortening of O−O distances[5] in the gibbsite sheet, leading to its curvature and hence to the formation of the imogolite NT. The lattice mismatch imposes an optimal curvature, which leads to the minimum strain in the structure[3,7] explaining its monodispersity and geometrical parameters. The imogolite structure is outstanding in this context, and other clay mineral NTs such as halloysite[8] and chrysotile[9] do not present similar behavior. Monodisperse NTs are attractive materials due to their vast range of potential applications that have been suggested for gas storage,[10,11] molecular sieves and adsorbents, inorganic catalyst support,[12] gas separation, transport of molecular species,[13] and coatings for nanowires.[14] Therefore, it is important to search for imogolite-like NTs that have different geometrical parameters, and thus offer a wider range of applications. The gibbsite sheet provides a template for developing other imogolite-like NTs as has been pointed out earlier.[15] Recently, on the basis of computational modeling, it has been shown that M-imogolite-like NTs (M = AsO_3, AsO_4, PO_3, and PO_4 fragments) are plausible structures in which the SiO_4 fragment was replaced.[16] The synthesis of an imogolite-like structure was reported by Wada and Wada[17] in 1982, who prepared an imogolite analogue replacing silicon by germanium atoms. This aluminogermanate NT (hereafter referred to as img-Ge, while img-Si will denote imogolite and the term "imogolites" the family of both materials) has a much shorter length (around 20 nm instead of hundreds of nanometers) and larger radii (outer radii around 20 Å) than img-Si.[18] Both syntheses, img-Si and img-Ge, occur in mild conditions in aqueous solution. The first synthesis of img-Si has been performed by Farmer et al.[19] in 1977. Ever since, synthesis

Received: November 11, 2013
Revised: February 19, 2014
Published: February 24, 2014

dx.doi.org/10.1021/jp411086f | J. Phys. Chem. C 2014, 118, 5945−5953

protocols for img-Si and img-Ge have been developed and described in the literature.[4,18,20−24]

It has been shown that img-Ge NTs can be obtained in large amount with reasonable formation kinetics at concentrated solution (decimolar).[25] According to Levard et al.,[24] the higher solubility of GeO_2 species in comparison to SiO_2 explains why img-Ge grows faster with higher initial reactant concentration than img-Si. Moreover, the synthesis process is sensitive to pH, concentration, and ionic strength. The control of such conditions will define the formation of single-walled (SW), double-walled (DW) img-Ge NT or even img-Ge hollow nanospheres.[26]

Recently, Maillet et al.[27] have shown that img-Ge NT can exist as SW or DW NTs, depending on the initial concentration of the reactants, a counterintuitive finding as it is well-known that the optimum curvature of img-Ge should define a NT with well-defined radius. However, if the initial aluminum perchlorate concentration is 0.25 mol·dm^{-3}, only DW NTs are formed, while at higher concentration (0.5 mol·dm^{-3}) SW NTs are obtained. On the basis of small-angle X-ray scattering (SAXS) and atomic force microscopy (AFM) images, Maillet et al.[23] have shown that the length distributions are much broader than the diameter distribution for DW and SW. The DW NTs have average radii of 15 ± 3 Å and length of 200 ± 150 Å, whereas the SW NTs are thinner (13 ± 3 Å) but significantly longer (500 Å). In addition, they report a distance of 2.7 Å between the Ge layer of the external tube and Al layer of internal, what indicates that no covalent bonds are present between the inner and outer walls of the DW NTs.

In order to understand the conditions allowing the formation of SW or DW img-Ge NTs, Thill et al.[21] explored the physicochemical conditions controlling the NT formation. They proposed a model in which the balance between attractive interaction energy and internal curvature energy of the initial protoimogolite explains the formation of one NT over the other. Besides, the effect of reactant concentration over SW or DW NTs formation should be related to the modification of the ionic strength. The change of ionic strength interferes with the electrostatic attractive energy between the initially formed protoimogolite moieties and thus directs synthesis to DW or SW NT.

Img-Si, img-Ge, and mixed $[(OH)_3Al_2O_3Si_xGe_{1-x}OH]$ SW NTs have been studied by Konduri et al.[28] using clay force field (CLAYFF)-based classical molecular dynamics simulations. The total internal energy per atom as a function of composition and diameter was plotted, showing energy minima in all cases. The minima shift gradually to higher diameters as Ge content increases.[28]

In the present work, we have investigated the stability, electronic, structural, and mechanical properties of SW and DW img-Ge NTs using the self-consistent charge density-functional tight-binding (SCC-DFTB) method. The *zigzag* and *armchair* chiralities have been investigated for SW img-Ge and img-Si NTs for comparison. In the case of DW NTs only the zigzag structures were investigated since they are significantly favored on energetic grounds.

COMPUTATIONAL DETAILS

The electronic structure calculations of SW and DW img-Ge NTs as well as the SW img-Si NTs were carried out using the self-consistent-charge density-functional tight-binding (SCC-DFTB) method.[29−31] This method uses a minimal, localized, and confined atomic basis set and tight-binding-like approximations to the Hamiltonian. The SCC-DFTB parameters for the Ge−X (X = Ge, O, Al, H) were evaluated following the protocol described in other works[3,9,31−34] (see the Supporting Information). The Framework for Automatization of SLAKO Parameterization (FASP) program,[35] developed in our research group, has been used to parametrize automatically the pairwise repulsion energy (E_{rep}) of the Ge−X (X = Ge, O, Al, H) atomic pairs. All the other SCC-DFTB parameters required to study img-Ge and img-SiNTs were those used in previous works.[3,8,16]

The initial NT structures have been built by rolling the two-dimensional (2D) layer of img-Ge using the same convention for labeling the carbon NTs, see Figure 1. The same is valid for

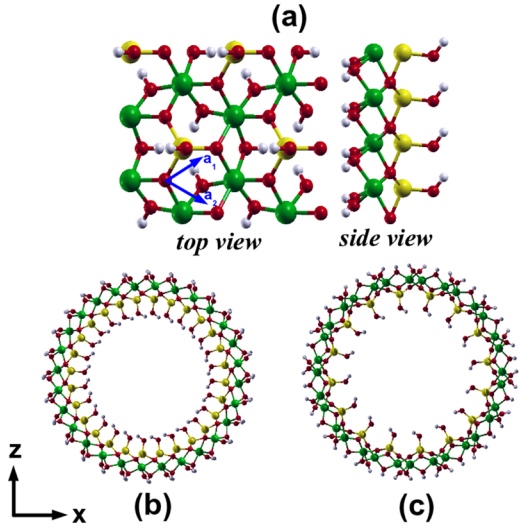

Figure 1. Top and side view of the layer used to generate the zigzag and armchair img-Ge nanotubes (a); view of the (14,0) zigzag (b) and (8,8) armchair (c) img-Ge nanotubes. Atom colors: Al, green; O, red; Ge, yellow; H, white.

building the img-Si NTs. Depending on the curling direction **B** in the 2D lattice $\mathbf{B} = n\mathbf{a}_1 + m\mathbf{a}_2$ ($\mathbf{a}_1$ and $\mathbf{a}_2$ are lattice vectors of the hexagonal lattice) three classes of NTs can be constructed: zigzag (n,0), armchair (n,n,) and chiral (n,m); the latter has $n \neq m$. The unit cell layer, with the chiral vectors $\mathbf{a}_1$ and $\mathbf{a}_2$, used to construct the NTs, are shown in Figure 1. The SW zigzag (n,0) (n = 9−19) and armchair (n,n) (n = 5−11) have been calculated.

The DW (p,0)@(q,0) img-Ge NTs were built from the fully optimized unit cell of the SW img-Ge NTs. The DW NTs were grouped in a way that the internal and external walls of the DW NTs were constructed from the SW (p,0) and (q,0) NTs ($p < q$), respectively. The following combination of NTs size were studied: (p,0)@(q,0), where $q - p$ = 8, 9, 10, 11.

The geometric parameters within the unit cells of all zigzag and armchair SW and DW img-Si and img-Ge NTs were fully optimized. Periodic boundary conditions were applied using the unit cell with the parameter a and c ($a = c$) set to be 100 Å, ensuring no spurious interaction between the individual tubes. The parameter b, along the y-direction (tube axis) was relaxed. The SW and DW img-Si NTs were calculated for comparison purpose following the same protocol.

We distinguish between internal and external radii of the imogolite NTs, which we define by the averaged distances of the inner and outer hydrogens to the cylinder axis, respectively. The intertubular distance d_{wall} is defined for the DW NTs as the

dx.doi.org/10.1021/jp411086f | J. Phys. Chem. C 2014, 118, 5945−5953

difference of the outer and inner hydrogen positions in the inner and outer NTs, see Scheme 1.

Scheme 1. Definition of the External and Internal Radii and the Distance between the Walls of the NTs

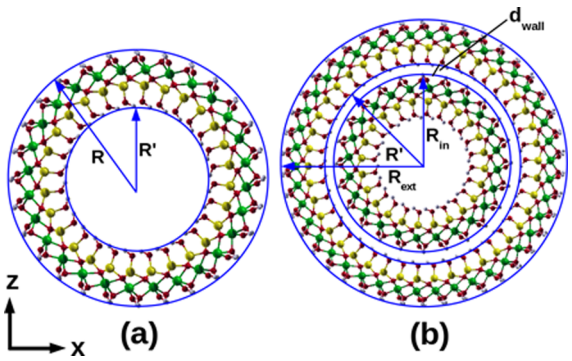

The mesh of points in k space[36] used to describe the first Brillouin zone was 1 × 6 × 1. All calculations have been performed using the DFTB+ program.[37] The electrostatic map was evaluated using the Visual Molecular Dynamics (VMD) software[38] together with the Adaptive Poisson−Boltzmann Solver (APBS) package[39] from the calculated SCC-DFTB Mulliken atomic charges.

RESULTS AND DISCUSSION

Single-Walled NTs. The strain energy of the SW img-Ge and img-Si NTs (E_{str}) is defined as the difference between the energy of the NT (E_{tube}) per number of atom (N_{tube}) present in its unit cell and the energy of the monolayer (E_{layer}) per number of atom present in its unit cell (N_{layer}), eq 1:

$$E_{str} = E_{tube} - E_{layer} \quad (1)$$

The strain energy is interpreted as the energy required for curling a planar sheet onto a cylinder. The strain energy curves for imogolite, halloysite, and chrysotile NT clay minerals have been reported in the literature.[3,8,9] The imogolites are special, as the strain energy curve presents a minimum. In contrast, other clay mineral NTs follow the same trend as carbon NTs, which decreases asymptotically to zero for large radii. The minimum in the strain energy curve explains the monodispersity and the well-defined img-Si and img-Ge NT structures with respect to its congeners. Two different DFT calculations, using B3LYP[40] and PBE[41] XC functional, led to the conclusion that the hydrogen-bond network in the inner side of the img-Si NT is important for the structure stabilization. The inner-side hydrogen-bond network certainly contributes to the stabilization of the img-Si and img-Ge. However, a theoretical analysis[16] has shown that this is not sufficient to explain the minimum in the strain energy curve. For instance, the arsenic and phosphorus imogolite-like structures also present a minimum in the strain energy curve but do not present an inner-side hydrogen-bond network. Nevertheless, the inner hydroxyl orientations seem to influence the strength of the hydrogen-bond network and the structure stabilization.

In order to elucidate the role of the inner hydrogen-bond network, we calculated three possible orientations of the inner hydroxyl groups to understand its influence on the stability of the zigzag and armchair SW img-Ge and img-Si NTs. The orientations are labeled according to the inner hydrogen orientations as follows: clockwise (img-X-1), anticlockwise (img-X-2), and both (img-X-3) directions (X = Si, Ge), see Figure 2. The strain energy dependence on the tube radius for

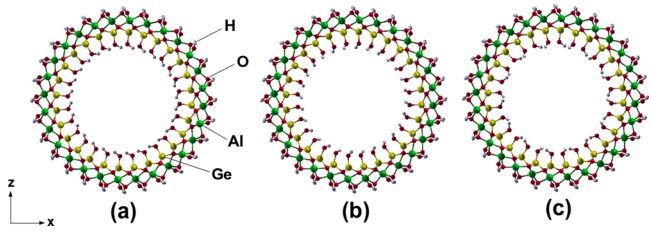

Figure 2. Optimized structure of (14,0) zigzag img-Ge nanotubes with the inner hydrogen atoms oriented to the clockwise (img-Ge-1) (a), anticlockwise (img-Ge-2) (b), and both (img-Ge-3) (c) directions. Atom colors: Al, green; O, red; Ge, yellow; H, white.

the img-Si and img-Ge tubes with the three orientations is presented in Supporting Information Figure S1. For img-Ge, the clockwise orientation (img-Ge-1) is the most stable one, being about 0.84 and 2.07 meV/atom lower in energy than img-Ge-3 and img-Ge-2, respectively. Also for the img-Si, the clockwise orientation is the most stable one, being about 0.71 meV/atom lower in energy than the anticlockwise orientation, although the relative stability changes for the external radii larger than 14 Å.

Figure 3 shows the comparison of the strain energy as a function of the tube radius (later on called strain energy curves)

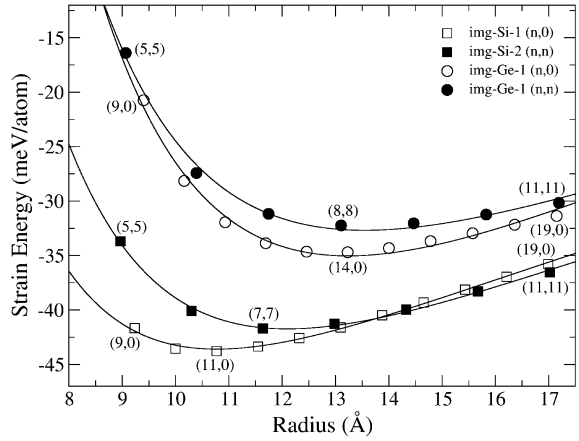

Figure 3. Strain energy per atom as a function of the outer tube radius for single-walled img-Si and img-Ge NTs: (9,0)−(19,0) zigzag (n,0) (opened squares and circles) and (5,5)−(11,11) armchair (n,n) (closed squares and circles). Img-Si are labeled by squares and img-Ge by circles. Only the most stable orientations of the inner hydroxyl are shown.

for the zigzag (n,0) and armchair (n,n) img-Si-1 and img-Ge-1 (hereafter img-Si and img-Ge) NTs. The strain energy curves of all studied NTs were fitted to eq 2, as suggested elsewhere,[3] in which R is the external NT radius, hereafter, for convenience simply called radii.

$$E_{str}(R) = \frac{a}{R^2} + \frac{b}{R} \quad (2)$$

The values of a and b coefficients for all calculated NTs and chiralities can be found in the Supporting Information.

The zigzag chirality is the most stable one in the whole range of radii investigated for img-Ge, and up to 14 Å for img-Si. This

dx.doi.org/10.1021/jp411086f | J. Phys. Chem. C 2014, 118, 5945−5953

Table 1. Experimental and Calculated Radii of the SW and DW img-Si, SW and DW img-Ge NTs

nanotube	method	radii (Å)	ref
SW img-Si	exptl	11.5	6
	PBE/DFT	8.75	7
	B3LYP/DFT	7.26[a]	40
	PBE/DFT	9.998	41
	SCC-DFTB	9.86	3
	SCC-DFTB	10.8	present work
DW img-Si	SCC-DFTB	9.25 (internal)/16.21 (external)	present work
SW img-Ge	exptl	16.5	17
		16.5	6
		15.02 ± 0.05	25
		15	42
		17.5 ± 0.8	27
		12.5 ± 2.5	23
		19	21
	SCC-DFTB	13.23	present work
DW img-Ge	exptl	12.0 ± 0.5 (internal)/20.0 ± 0.5 (external)	27
		15.0 ± 2.5 (external)	23
		13 (internal)/21.5 (external)	21
	SCC-DFTB	11.71 (internal)/18.73 (external)	present work

[a]Internal diameter. The external radii can be roughly estimated to be 10 Å.

appears to be another specific property, so far only observed in imogolites. For the inorganic NTs such as chrysotile[9] and halloysite,[8] the strain energy curves are not affected by their chiralities. The minima in the strain energy curves occur at external radii of 10.8 (11,0) Å and 13.2 (14,0) Å for img-Si and img-Ge, respectively. The radii increase with the replacement of the silicon by germanium is expected. In experiment, this difference is higher with a value of about 5 Å.[17,25,42] A comparison to the available experimental and other calculated radii for the img-Si and img-Ge is shown at Table 1. One has to be aware that we are calculating idealized structures while the img-Ge and img-Si syntheses occur in aqueous solution, thermodynamically controlled by temperature, pH, and ionic strength. Recently, Yucelen et al.[20] have shown that the NT radii can be controlled by the electrolyte used to set the ionic strength and the radii can change up to 4 Å. The role of the solution pH and ionic strength in the formation of the protoimogolite and the subsequent self-organization to form the NTs remains to be understood. Furthermore, the radii have not been calculated using the same definition: our definition is based on the outer hydrogen layer that should naturally limit the tube; in experiment, the radii are determined by the analysis of microscopic data, where highest diffraction is expected at the heavier atoms, and thus the tubes are associated with smaller radii.

The optimized cell parameters b of the SW (14,0) zigzag img-Ge and (11,0) zigzag img-Si NTs are 8.64 and 8.56 Å, respectively. Thus, the length difference per formula unit along the tube axis between the most stable img-Ge and img-Si NTs is very small, only 0.08 Å, indicating that the unit cell length along the tube axis is not much affected by the silicon replacement.

The average Ge−Ge and Ge−Al distances for the (14,0) img-Ge NT are 4.61 and 3.28 Å, respectively. These values are, respectively, 0.12 and 0.09 Å larger than the Si−Si and Si−Al distances in the (11,0) img-Si NTs. The Ge−O and Ge−Al interatomic distances of 1.74 and 3.28 Å for the zigzag (14,0) NT are in agreement with the extended X-ray absorption fine structure (EXAFS)[42] estimates of 1.75 and 3.26 Å, respectively. As discussed by Levard et al.,[42] the shorter O−O distances in the Ge tetrahedron (∼2.78 Å) compared to the Al dioctahedral (gibbsite) vacancy (∼3.2 Å) explains the curvature of the img-Ge NTs. This is in line with our calculated O−O distances in the Si tetrahedron of (11,0) img-Si NT, which is shorter (2.67 Å) than that of (14,0) img-Ge (2.78 Å), explaining the larger radii found for the img-Ge NTs.

Double-Walled NTs. Maillet et al.[27] have shown the first evidence of the DW img-Ge formation. Recently, details of the physicochemical control over the single- and double-walled img-Ge NTs have been provided,[21,23] indicating that DW NTs are also thermodynamic products and, hence, the radii of the inner and outer NTs can be modified with respect to the SW NTs. We have used the optimized SW img-Ge NTs to construct the $(p,0)@(q,0)$ DW NTs for p = 10−16 and $q-p$ = 8−11. The external radii of the inner NTs (R_{in}), the external radii of the outer NTs (R_{ext}), the distances between the walls (d_{wall}), and the electronic band gaps (BG) of the fully optimized DW NTs are shown at Table 2. More details are given in Table S3 at the Supporting Information.

In order to determine the relative orientation of the two tubes with respect to each other, the internal NT was rotated along the tube axis with respect to the external tube. The curves are shown in Figure S2 (Supporting Information), indicating that the rotation accounts for differences of up to 1.4 meV/atom.

The best configuration for the internal NT is at the center of the external NT. Tests to translate it slightly to different directions resulted in an increase of the strain energy as shown in Figure S3 (Supporting Information).

The strain energy curve for the DW img-Ge as function of the outermost radii is shown in Figure 4. The bilayer was used as reference for estimating E_{layer} in eq 1. Each point of the strain energy curve corresponds to the minimum of the $(p,0)@(q,0)$ ($p-q$ = 8−11) NTs. The curve was fitted using eq 2 (see the Supporting Information for more details). For all DW NTs studied here the most stable configurations are the ones with $q - p = 9$. d_{wall} is in the range of 1.40−1.51 Å, thus favoring the stabilization of the DW NTs through hydrogen bonds. The

dx.doi.org/10.1021/jp411086f | J. Phys. Chem. C 2014, 118, 5945−5953

Table 2. Outer Radii of the Internal (R_{in}) and External (R_{ext}) DW img-Ge and img-Si NTs, Distances between the Walls (d_{wall}), and Band Gaps (BG)

	R_{in} (Å)	R_{ext} (Å)	d_{wall} (Å)	BG (eV)
img-Ge				
(10,0)@(19,00)	10.16	17.16	1.40	8.5
(11,0)@(20,00)	10.94	17.95	1.42	8.5
(12,0)@(21,00)	11.71	18.73	1.43	8.5
(13,0)@(22,00)	12.46	19.54	1.49	8.5
(14,0)@(23,00)	13.24	20.32	1.51	8.6
(15,0)@(24,00)	14.02	21.11	1.51	8.6
(16,0)@(25,00)	14.80	21.89	1.51	8.6
img-Si				
(07,0)@(16,00)	7.79	14.65	1.55	7.9
(08,0)@(17,00)	8.50	15.44	2.05	8.0
(09,0)@(18,00)	9.25	16.21	2.07	8.0
(10,0)@(19,00)	10.01	16.98	2.09	8.1
(11,0)@(20,00)	10.79	17.76	2.10	8.2
(12,0)@(21,00)	11.57	18.53	2.10	8.2
(13,0)@(22,00)	12.35	19.31	2.10	8.3

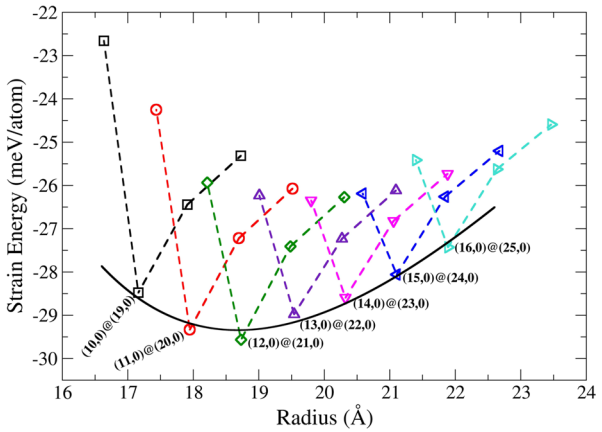

Figure 4. Strain energy per atom as a function of the outer radius for double-walled (p,0)@(q,0) img-Ge NTs taking into account different sizes and walls interactions: $q - p$ = 8, 9, 10, and 11. Dashed lines are related to the same inner NT but different outer NTs. The reference used to calculate the double-walled NTs strain energies has been the bilayer.

(12,0)@(21,0) DW NT is the most stable one, with the inner and outer radii of 11.71 and 18.73 Å, respectively (Figure 5). Thill and co-workers[21,27] estimated the external radii of the internal and external NTs by imposing their SAXS data on an

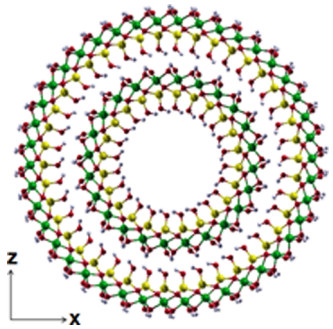

Figure 5. Structure of the double-walled (12,0)@(21,0) img-Ge nanotube.

open cylindrical structure model. The values for internal NT radii are in the range of 12.0−13.0 Å, and those for the external NT are in the range of 20−21.5 Å. The calculated difference of 7.02 Å between the external walls must be compared to the experimental estimated value of 8.5 Å. The SCC-DFTB calculated NTs seem to overestimate the bond strength leading to smaller radii, about 1−2 Å. Maillet et al.[27] also estimated the average distance between the external and internal NTs based on a simple model of two cylinders. They interpreted the value of 2.7 Å to be the interatomic distance between the Ge sheet of the external NT and the Al sheet of the internal NT. However, this value seems to be too small if one takes into account the hydroxyls bound to the Ge and Al atoms of the two tubes. Our estimated value is about 5.4 Å. We have also calculated the interatomic distances between the oxygens of the hydroxyls bound to the Ge atoms of the outer NT and the oxygens of the hydroxyls bound to the Al atoms of the inner NT, obtaining a value of 2.67 Å. Thus, the experimental value of 2.7 Å between the two tubes is better interpreted as the interatomic distances between the two oxygen sheets bound to the Ge and Al atoms.

One could argue that the inclusion of London dispersion, for example, as proposed by Zhechkov et al.,[43] is important to correctly describe the strain energy of the DW NTs due to their contribution to the interlayer stabilization energy. Therefore, strain energy curve for the DW img-Ge tubes has been calculated including the dispersion correction. The result is shown in Supporting Information Figure S4 and has similar behavior. The most stable (p,0)@(q,0) configurations are also for $q - p$ = 9. The curve shows a general stabilization by 0.06 meV/atom with respect to the bilayer. The difference of the relative energy of the different configurations is less than 0.01 meV/atom, indicating that electrostatic interactions govern the interlayer interactions.

The optimized cell parameter b for the (12,0)@(21,0) img-Ge NT is 8.64 Å, which is very similar to the SW (14,0) img-Ge NTs. The structural properties of the DW (12,0)@(21,0) NT did not change significantly compared to that of (14,0) img-Ge NT. The Ge−Ge and Ge−Al interatomic distances are about 0.06 and 0.01 Å larger with respect to the (14,0) NT, respectively, indicating that the DW NT formation does not affect significantly its structure.

It is important to highlight that the most stable SW (14,0) img-Ge is not involved in the DW (12,0)@(21,0) NT. This is expected since the img-Ge formation is thermodynamically controlled leading to the most stable structure. Actually, the sum of the strain energies of the SW (12,0) and SW (21,0) is 0.59 meV/atom smaller than the sum of the SW (14,0) and (23,0) NTs. For larger radii, the Ge−O−Al bonding is strengthened and the (12,0)@(21,0) is the best combination. The formation energy from the SW NTs to the DW img-Ge NTs is estimated to be −2.48 meV/atom. In the case of the (14,0)@(23,0), the formation energy is about −2.10 meV/atom, indicating that the hydrogen bonding is also more favorable for the (12,0)@(21,0) DW NT.

The hypothetical DW img-Si NTs have also been calculated and the strain energy curve is depicted in Supporting Information Figure S5, showing the same trend as for the DW img-Ge. The most stable DW NT is the (9,0)@(18,0) one, showing that the combination $p-q$ = 9 is the best for both img-Si and img-Ge DW NTs. Figure 6 shows a comparison between the SW and DW NTs for the img-Si and img-Ge systems. The SW and DW curves get close to each other for larger radii. One has to take into account that the strain energy of the DW NTs

dx.doi.org/10.1021/jp411086f | J. Phys. Chem. C 2014, 118, 5945−5953

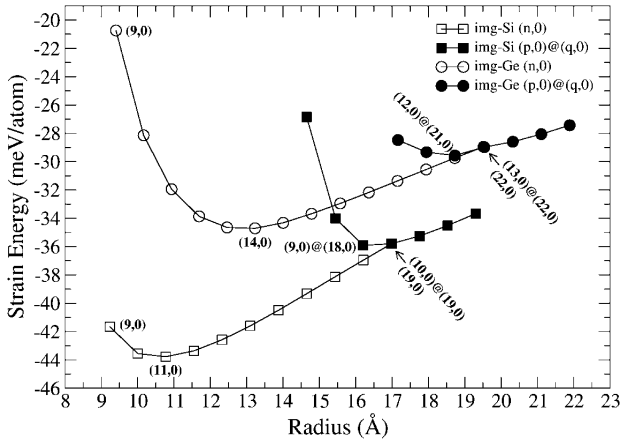

Figure 6. Strain energy curves for the SW and DW NTs of the img-Si and img-Ge systems.

is defined taking the respective bilayer as reference; thus, the interaction between the inner and outer NTs are already included. Therefore, for larger radii the SW and DW curves get closer. For the smaller radii, the strain energy contribution of the inner NT increases drastically. Our findings corroborate with the energy-based model proposed by Thill et al.[21] Flexible protoimogolite thin sheets have spontaneous curvature, and depending on the pH and ionic strength of the solution, the surfaces are charged. Two sheets can be attracted by electrostatic interaction. In their proposal, the double-walled structure will be formed if the bending energy still keeps the systems favored. For the DW (9,0)@(18,0) img-Si NT, the inner NT presents a large strain energy compared to the most stable (11,0) img-Si; thus, it is not favoring the DW formation. However, for the DW (12,0)@(21,0) img-Ge, the inner NT presents relatively small increase of the strain energy with respect to the most stable SW (14,0) img-Ge NT. The formation energy of the DW (9,0)@(18,0) img-Si NT is estimated to be −1.74 meV/atom with respect to the respective SW NTs. This value is about 0.74 meV/atom larger than for DW img-Ge probably due to smaller interaction between the two tubes through hydrogen bonding. It is also important to note that d_{wall} is estimated to be 1.43 and 2.07 Å for the DW (12,0)@(21,0) img-Ge and (9,0)@(18,0) img-Si NTs, respectively. Therefore, it is expected that the hydrogen bonding at the DW img-Ge is more favorable than the DW img-Si.

Electronic Properties. The calculated electronic band gaps (BG) for all SW img-Ge NTs with the respective external radius are shown in Table 3. These quantities are insensitive to the orientation of the hydrogen-bonding network at the inner side of the NTs as one can observe from Supporting Information Tables S1 and S2. The BG is in the range of 9.5−9.8 and 10.2−10.6 eV for the img-Ge and img-Si, respectively, showing that both NTs are insulators. The BGs for img-Si calculated at the GGA-DFT level are in the range of 4.7−5.2 eV,[7,44] and the previously published SCC-DFTB values are about 10 eV.[3] As has been pointed out elsewhere,[3] it is generally accepted that DFTB overestimates and GGA-DFT underestimates the band gaps, so one can safely conclude that these materials are high band gap insulators.

Total and partial density of states (PDOS) of the SW (14,0) zigzag, SW (8,8) armchair, and DW (12,0)@(21,0) img-Ge structures are presented in Supporting Information Figure S7.

Table 3. Number of Atoms in the Unit Cell (N), Outer Radii (R), Band Gap (BG), and Young's Modulus (Y) of the Single-Walled (9,0)−(19,0) Zigzag and (5,5)−(11,11) Armchair img-Ge Nanotubes

type	N	R (Å)	BG (eV)	Y (GPa)
Zigzag (n,0)				
(9,0)	252	9.40	9.5	350
(10,0)	280	10.16	9.5	348
(11,0)	308	10.93	9.6	346
(12,0)	336	11.69	9.6	343
(13,0)	364	12.46	9.6	340
(14,0)	392	13.23	9.5	337
(15,0)	420	14.00	9.5	333
(16,0)	448	14.78	9.5	327
(17,0)	476	15.57	9.5	323
(18,0)	504	16.36	9.5	322
(19,0)	532	17.15	9.5	320
Armchair (n,n)				
(5,5)	140	9.07	9.6	370
(6,6)	168	10.40	9.6	359
(7,7)	196	11.75	9.6	351
(8,8)	224	13.11	9.6	345
(9,9)	252	14.47	9.6	340
(10,10)	280	15.83	9.6	336
(11,11)	308	17.19	9.6	332
layer	28		9.2	

At the Fermi level, the valence band is governed by oxygen states. The largest contribution to the conduction band arises from the germanium atoms. The img-Ge PDOS is very similar to the img-Si PDOS, as shown in Supporting Information Figure S6, with the largest contribution of the oxygen and silicon states to the valence and conduction bands, respectively. It is interesting to observe that the PDOS is also very similar to img-As-ate and img-P-ate,[16] which implies that even when the silicon is replaced by other atoms that do not belong to the same main group of the periodic table and that carry larger oxidation numbers, the electronic structure remains similar. The band gaps for the img-As-ate and img-P-ate are about 7.5 and 10 eV. However, for the img-As-ite and img-P-ite, where the As and P atoms have lower oxidation numbers, the band gaps are much smaller and in the range of 4.8−5.2 eV at the SCC-DFTB level of theory. Furthermore, the shape of the electronic DOS presents some changes near the Fermi level with respect to the other imogolite-like structures.

The PDOS of the DW (12,0)@(21,0) img-Ge NT is very similar to the respective SW NTs (see Supporting Information Figure S7). The BG of the DW NTs are about 1 eV smaller than the respective SW NTs with a value of 8.5 eV.

The SCC-DFTB Mulliken charges do not change significantly with respect to the chirality and size of the system. The Al and Ge atoms in the img-Ge NTs present +0.35e and +0.61e, respectively. In corresponding charges in img-Si NTs are for Al and Si about +0.37e and +0.57e, respectively. Furthermore, the O atoms bound to Al and Ge have a net charge of −0.32e and −0.39e, respectively. For img-Si, the O atoms bound to Al and Si had a net charge of −0.33e and −0.43e, respectively. In comparison to the DW (12,0)@(21,0) img-Ge NT, the Al and Ge charges are not changed significantly with respect to the (14,0) img-Ge NT.

The electrostatic maps obtained from SCC-DFTB Mulliken charges for img-Ge and img-Si NTs are shown in the Figure 7

dx.doi.org/10.1021/jp411086f | J. Phys. Chem. C 2014, 118, 5945−5953

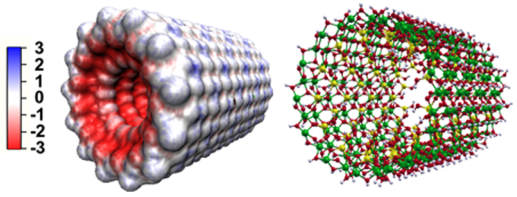

Figure 7. Electrostatic field and the structure of the single-walled (14,0) zigzag img-Ge nanotubes. The scale of the colors surfaces is in 25.7 mV.

and Supporting Information Figure S8, respectively. The charge distribution of img-Ge and img-Si NTs shows strongly negative and weakly positive charges on the inner and outer surfaces, respectively.

Mechanical Properties. The mechanical properties of clay minerals are very important for technological applications. In the present study, the Young moduli (Y) have been estimated using eq 3, in which ε is the strain in the vicinities around the optimum lattice vector and E is the total energy. V_0 is the equilibrium volume of the tube, which is evaluated by the cylinder equation: $V_0 = \pi C_0(R_{out}^2 - R_{in}^2)$, C_0 is the cell length, R_{out} is the outer radius, and R_{in} is the inner radius: The Young modulus was estimated using numerical derivatives.

$$Y = \frac{1}{V_0}\left(\frac{\partial^2 E}{\partial \varepsilon^2}\right)_{\varepsilon=0} \quad (3)$$

The estimates of the Young moduli of the zigzag and armchair SW img-Ge NTs are shown in Table 3. The Young moduli are in the range of 320−370 GPa for both img-Ge and img-Si NTs (see Tables S1 and S2). The Young modulus of the DW (12,0)@(21,0) NT is calculated to be 328 GPa, close to the (14,0) value of 337 GPa. This is expected since the DW NTs do not change the bonding character or structure of the NTs. The range of the Young moduli of the SW and DW img-Ge NTs are in the same order of magnitude than other inorganic NTs such as img-Si (∼175−390 GPa),[3] halloysite (∼230−240 GPa),[8] chrysotile (∼261−323),[9] WS_2 (∼230 GPa),[45] and GaS (∼270 GPa).[46]

FINAL REMARKS

SW and DW imogolites (img-Ge and img-Si) NTs have been investigated using the SCC-DFTB method. The orientation of the internal hydroxyls forming hydrogen bonding has been addressed and it affects slightly the strain energy curves of SW NTs. The band gaps and Young moduli are not affected by the orientation of the hydrogen atoms in the NT inner side. The strain energy curves for the SW img-Ge NTs indicated the (14,0) zigzag NT as the most stable with the external radii of 13.23 Å which must be compared to the experimental values of 13 ± 3 Å.[23] The DW (p,0)@(q,0) NTs with $q-p$ = 9 are the most stable structures probably due to the hydrogen-bonding maximization between the walls of the NTs and the smaller sum of the strain energies of the NTs. The energetically most stable structure is the (12,0)@(21,0) with external radii estimated to be 18.73 Å, which is in reasonable agreement with the experimental value of 15.2 ± 3 Å.[23]

The hypothetical DW img-Si follow the same behavior as DW img-Ge, with $q-p$ = 9 as the most stable configurations. The strain energy curve presents a minimum and the DW (9,0)@(18,0) is the most stable structure with external radii estimated to be 16.21 Å. The strain energy difference between SW (11,0) and DW (9,0)@(18,0) img-Si is about 7.86 meV/atom and the intertubular interaction is only −1.74 meV/atom. These results must be compared to the strain energy difference between SW (14,0) and DW (12,0)@(21,0) img-Ge of only 5.14 meV/atom and the intertubular interaction of −2.48 meV/atom. The larger strain energy difference and the low intertubular interaction explain why DW img-Si is not favored compared to the DW img-Ge.

The density of states indicate that both structure are insulators and the band gap of the DW is about 1 eV smaller than the SW at the SCC-DFTB level of theory. The NT outer surface are slightly positive and the NT inner surface are negative. The SW and DW NTs Young moduli are in the range of 320−370 GPa, which is in the same order as other inorganic and natural NTs.

The control of the length, radii, and the formation of SW or DW imogolite-like structures as it has been shown recently are interesting.[20,21] However, the molecular modeling of the formation mechanism at a molecular level is still challenging. The influence of the water solvent, ionic strength, electrolyte, and pH is very crucial. The chemical speciation during the synthesis have been investigated quite intensely;[23,24,42] however, the chemical condition for the synthesis of other imogolite-like structures as proposed elsewhere seem to be a question of time.

In conclusion, our calculations rationalize the existence of double-walled imogolite-like nanotubes and indicate that the electrostatic interactions between layers and between layer and solvent have a significant influence on the curvature of the tubes, thus defining their diameters. Our calculations suggest that imogolite-like nanotubes of tailored diameter can be formed, depending on composition and synthesis conditions. Those can be well-defined templates, for example, for the formation of other nanostructures or as selective molecular sieves.

ASSOCIATED CONTENT

Supporting Information

Details of the SCC-DFTB parametrization of the atomic pairs GeX (X = Ge, O, Al, H), strain energy, electronic, structural, and mechanical properties of all studied zigzag and armchair img-Ge/Si-1, img-Ge/Si-2, and img-Ge/Si-3 NTs, strain energy and structural properties of the DW img-Ge NTs, strain energy of the DW (p,0)@(q,0) NTs as a function of the rotation and translation of the internal (p,0) NT, fitting of the strain energy of the SW and DW NTs, PDOS and electrostatic map of zigzag and armchair img-Ge and img-Si NTs, PDOS of the DW (11,0)@(21,0) img-Ge NT, diffractograms of the SW and DW img-Ge, and strain energy curves for the DW img-Ge including the dispersion correction. This material is available free of charge via the Internet at http://pubs.acs.org.

AUTHOR INFORMATION

Corresponding Author

*E-mail: duarteh@ufmg.br.

Notes

The authors declare no competing financial interest.

ACKNOWLEDGMENTS

The support of the Brazilian agencies Fundação de Amparo à Pesquisa do Estado de Minas Gerais (FAPEMIG), Conselho Nacional para o Desenvolvimento Científico e Tecnológico

(CNPq), and Coordenação de Aperfeiçoamento de Pessoal de Ensino Superior (CAPES) is gratefully acknowledged. The National Institute of Science and Technology has also funded this work for Mineral Resources, Water and Biodiversity—ACQUA-INCT (http://www.acqua-inct.org). Financial support of Deutsche Forschungsgemeinschaft (DFG, HE 3543/17-1) and the European Commission FP7Marie Curie TEMM1P PIRSES-GA-2011-295172 is gratefully acknowledged.

REFERENCES

(1) Ma, Z.; Wang, J.; Gao, X.; Ding, T.; Qin, Y. Application of Halloysite Nanotubes. *Prog. Chem.* **2012**, *24* (2−3), 275−283.
(2) Gustafsson, J. P. The Surface Chemistry of Imogolite. *Clays Clay Miner.* **2001**, *49* (1), 73−80.
(3) Guimaraes, L.; Enyashin, A. N.; Frenzel, J.; Heine, T.; Duarte, H. A.; Seifert, G. Imogolite Nanotubes: Stability, Electronic, and Mechanical Properties. *ACS Nano* **2007**, *1* (4), 362−368.
(4) Levard, C.; Masion, A.; Rose, J.; Doelsch, E.; Borschneck, D.; Dominici, C.; Ziarelli, F.; Bottero, J. Y. Synthesis of Imogolite Fibers from Decimolar Concentration at Low Temperature and Ambient Pressure: A Promising Route for Inexpensive Nanotubes. *J. Am. Chem. Soc.* **2009**, *131* (47), 17080−17080.
(5) Cradwick, P. D.; Wada, K.; Russell, J. D.; Yoshinag., N.; Masson, C. R.; Farmer, V. C. Imogolite, a Hydrated Aluminum Silicate of Tubular Structure. *Nature (London), Phys. Sci.* **1972**, *240* (104), 187.
(6) Mukherjee, S.; Bartlow, V. M.; Nair, S. Phenomenology of the Growth of Single-Walled Aluminosilicate and Aluminogermanate Nanotubes of Precise Dimensions. *Chem. Mater.* **2005**, *17* (20), 4900−4909.
(7) Zhao, M.; Xia, Y.; Mei, L. Energetic Minimum Structures of Imogolite Nanotubes: A First-Principles Prediction. *J. Phys. Chem. C* **2009**, *113* (33), 14834−14837.
(8) Guimaraes, L.; Enyashin, A. N.; Seifert, G.; Duarte, H. A. Structural, Electronic, and Mechanical Properties of Single-Walled Halloysite Nanotube Models. *J. Phys. Chem. C* **2010**, *114* (26), 11358−11363.
(9) Lourenço, M. P.; de Oliveira, C.; Oliveira, A. F.; Guimarães, L.; Duarte, H. A. Structural, Electronic, and Mechanical Properties of Single-Walled Chrysotile Nanotube Models. *J. Phys. Chem. C* **2012**, *116* (17), 9405−9411.
(10) Ackerman, W. C.; Smith, D. M.; Huling, J. C.; Kim, Y. W.; Bailey, J. K.; Brinker, C. J. Gas Vapor Adsorption in Imogolite: a Microporous Tubular Aluminosilicate. *Langmuir* **1993**, *9* (4), 1051−1057.
(11) Bottero, I.; Bonelli, B.; Ashbrook, S. E.; Wright, P. A.; Zhou, W.; Tagliabue, M.; Armandi, M.; Garrone, E. Synthesis and Characterization of Hybrid Organic/Inorganic Nanotubes of the Imogolite Type and Their Behaviour Towards Methane Adsorption. *Phys. Chem. Chem. Phys.* **2011**, *13* (2), 744−750.
(12) Nakagaki, S.; Wypych, F. Nanofibrous and Nanotubular Supports for the Immobilization of Metalloporphyrins as Oxidation Catalysts. *J. Colloid Interface Sci.* **2007**, *315* (1), 142−157.
(13) Dvoyashkin, M.; Zang, J.; Yucelen, G. I.; Katihar, A.; Nair, S.; Sholl, D. S.; Bowers, C. R.; Vasenkov, S. Diffusion of Tetrafluoromethane in Single-Walled Aluminosilicate Nanotubes: Pulsed Field Gradient Nmr and Molecular Dynamics Simulations. *J. Phys. Chem. C* **2012**, *116* (40), 21350−21355.
(14) Kuc, A.; Heine, T. Shielding Nanowires and Nanotubes with Imogolite: A Route to Nanocables. *Adv. Mater.* **2009**, *21* (43), 4353−4356.
(15) Duarte, H. A.; Lourenco, M. P.; Heine, T.; Guimaraes, L., Clay Mineral Nanotubes: Stability, Structure and Properties. In *Stoichiometry and Materials Science—When Numbers Matter*; Innocenti, A., Kamarulzaman, N., Eds.; InTech: Rijeka, Croatia, 2012; 3−24.
(16) Guimaraes, L.; Pinto, Y. N.; Lourenco, M. P.; Duarte, H. A. Imogolite-Like Nanotubes: Structure, Stability, Electronic and Mechanical Properties of the Phosphorous and Arsenic Derivatives. *Phys. Chem. Chem. Phys.* **2013**, *15* (12), 4303−4309.
(17) Wada, S.; Wada, K. Effects of Substitution of Germanium for Silicon in Imogolite. *Clays Clay Miner.* **1982**, *30* (2), 123−128.
(18) Thill, A.; Guiose, B.; Bacia-Verloop, M.; Geertsen, V.; Belloni, L. How the Diameter and Structure of $(OH)_3Al_2O_3Si_xGe_{1-x}OH$ Imogolite Nanotubes Are Controlled by an Adhesion Versus Curvature Competition. *J. Phys. Chem. C* **2012**, *116*, 26841−26849.
(19) Farmer, V. C.; Fraser, A. R.; Tait, J. M. Synthesis of Imogolite:A Tubular Aluminium Silicate Polymer. *J. Chem. Soc., Chem. Commun.* **1977**, 462−463.
(20) Yucelen, G. I.; Kang, D.-Y.; Guerrero-Ferreira, R. C.; Wright, E. R.; Beckham, H. W.; Nair, S. Shaping Single-Walled Metal Oxide Nanotubes from Precursors of Controlled Curvature. *Nano Lett.* **2012**, *12* (2), 827−832.
(21) Thill, A.; Maillet, P.; Guiose, B.; Spalla, O.; Belloni, L.; Chaurand, P.; Auffan, M.; Olivi, L.; Rose, J. Physico-Chemical Control over the Single- or Double-Wall Structure of Aluminogermanate Imogolite-Like Nanotubes. *J. Am. Chem. Soc.* **2012**, *134* (8), 3780−3786.
(22) Yucelen, G. I.; Choudhury, R. P.; Vyalikh, A.; Scheler, U.; Beckham, H. W.; Nair, S. Formation of Single-Walled Aluminosilicate Nanotubes from Molecular Precursors and Curved Nanoscale Intermediates. *J. Am. Chem. Soc.* **2011**, *133* (14), 5397−5412.
(23) Maillet, P.; Levard, C.; Spalla, O.; Masion, A.; Rose, J.; Thill, A. Growth Kinetic of Single and Double-Walled Aluminogermanate Imogolite-Like Nanotubes: An Experimental and Modeling Approach. *Phys. Chem. Chem. Phys.* **2011**, *13* (7), 2682−2689.
(24) Levard, C.; Masion, A.; Rose, J.; Doelsch, E.; Borschneck, D.; Olivi, L.; Chaurand, P.; Dominici, C.; Ziarelli, F.; Thill, A.; Maillet, P.; Bottero, J. Y. Synthesis of Ge-Imogolite: Influence of the Hydrolysis Ratio on the Structure of the Nanotubes. *Phys. Chem. Chem. Phys.* **2011**, *13* (32), 14516−14522.
(25) Levard, C.; Rose, J.; Masion, A.; Doelsch, E.; Borschneck, D.; Olivi, L.; Dominici, C.; Grauby, O.; Woicik, J. C.; Bottero, J.-Y. Synthesis of Large Quantities of Single-Walled Aluminogermanate Nanotube. *J. Am. Chem. Soc.* **2008**, *130* (18), 5862−5863.
(26) Bac, B. H.; Song, Y.; Kim, M. H.; Lee, Y.-B.; Kang, I. M. Single-Walled Hollow Nanospheres Assembled from the Aluminogermanate Precursors. *Chem. Commun.* **2009**, No. 38, 5740−5742.
(27) Maillet, P.; Levard, C.; Larquet, E.; Mariet, C.; Spalla, O.; Menguy, N.; Masion, A.; Doelsch, E.; Rose, J.; Thill, A. Evidence of Double-Walled Al−Ge Imogolite-Like Nanotubes. A Cryo-Tem and Saxs Investigation. *J. Am. Chem. Soc.* **2010**, *132* (4), 1208−1209.
(28) Konduri, S.; Mukherjee, S.; Nair, S. Controlling Nanotube Dimensions: Correlation between Composition, Diameter, and Internal Energy of Single-Walled Mixed Oxide Nanotubes. *ACS Nano* **2007**, *1* (5), 393−402.
(29) Elstner, M.; Porezag, D.; Jungnickel, G.; Elsner, J.; Haugk, M.; Frauenheim, T.; Suhai, S.; Seifert, G. Self-Consistent-Charge Density-Functional Tight-Binding Method for Simulations of Complex Materials Properties. *Phys. Rev. B* **1998**, *58* (11), 7260−7268.
(30) Frauenheim, T.; Seifert, G.; Elstner, M.; Hajnal, Z.; Jungnickel, G.; Porezag, D.; Suhai, S.; Scholz, R. A Self-Consistent Charge Density-Functional Based Tight-Binding Method for Predictive Materials Simulations in Physics, Chemistry and Biology. *Phys. Status Solidi B* **2000**, *217* (1), 41−62.
(31) Oliveira, A. F.; Seifert, G.; Heine, T.; Duarte, H. A. Density-Functional Based Tight-Binding: An Approximate Dft Method. *J. Braz. Chem. Soc.* **2009**, *20* (7), 1193−1205.
(32) Dolgonos, G.; Aradi, B. l.; Moreira, N. H.; Frauenheim, T. An Improved Self-Consistent-Charge Density-Functional Tight-Binding (Scc-Dftb) Set of Parameters for Simulation of Bulk and Molecular Systems Involving Titanium. *J. Chem. Theory Comput.* **2009**, *6* (1), 266−278.
(33) Koskinen, P.; Makinen, V. Density-Functional Tight-Binding for Beginners. *Comput. Mater. Sci.* **2009**, *47* (1), 237−253.
(34) Frenzel, J.; Oliveira, A. F.; Duarte, H. A.; Heine, T.; Seifert, G. Structural and Electronic Properties of Bulk Gibbsite and Gibbsite Surfaces. *J. Inorg. Gen. Chem.* **2005**, *631* (6−7), 1267−1271.

(35) Lourenco, M. P. Simulação Computacional das Propriedades Eletrônicas, Estruturais e Mecânicas de Nanotubos Inorgânicos. Ph.D. Thesis, Universidade Federal de Minas Gerais, Belo Horizonte, 2013; http://www.qui.ufmg.br/~duarteh/teses/Tese-Maicon_P_Lourenco.pdf.
(36) Monkhorst, H. J.; Pack, J. D. Special Points for Brillouin-Zone Integrations. *Phys. Rev. B* **1976**, *13* (12), 5188−5192.
(37) Aradi, B.; Hourahine, B.; Frauenheim, T. Dftb+, a Sparse Matrix-Based Implementation of the Dftb Method. *J. Phys. Chem. A* **2007**, *111* (26), 5678−5684.
(38) Humphrey, W.; Dalke, A.; Schulten, K. Vmd—Visual Molecular Dynamics. *J. Mol. Graphics* **1996**, *14*, 33−38.
(39) Baker, N. A.; Sept, D.; Joseph, S.; Holst, M. J.; McCammon, J. A. Electrostatics of Nanosystems: Application to Microtubules and the Ribosome. *Proc. Natl. Acad. Sci. U.S.A.* **2001**, *98* (18), 10037−10041.
(40) Demichelis, R.; Noel, Y.; D'Arco, P.; Maschio, L.; Orlando, R.; Dovesi, R. Structure and Energetics of Imogolite: A Quantum Mechanical Ab Initio Study with B3lyp Hybrid Functional. *J. Mater. Chem.* **2010**, *20* (46), 10417−10425.
(41) Lee, S. U.; Choi, Y. C.; Youm, S. G.; Sohn, D. Origin of the Strain Energy Minimum in Imogolite Nanotubes. *J. Phys. Chem. C* **2011**, *115* (13), 5226−5231.
(42) Levard, C.; Rose, J.; Thill, A.; Masion, A.; Doelsch, E.; Maillet, P.; Spalla, O.; Olivi, L.; Cognigni, A.; Ziarelli, F.; Bottero, J. Y. Formation and Growth Mechanisms of Imogolite-Like Aluminogermanate Nanotubes. *Chem. Mater.* **2010**, *22* (8), 2466−2473.
(43) Zhechkov, L.; Heine, T.; Patchkovskii, S.; Seifert, G.; Duarte, H. A. An Efficient a Posteriori Treatment for Dispersion Interaction in Density-Functional-Based Tight Binding. *J. Chem. Theory Comput.* **2005**, *1* (5), 841−847.
(44) Alvarez-Ramirez, F. Ab Initio Simulation of the Structural and Electronic Properties of Aluminosilicate and Aluminogermanate Natotubes with Imogolite-Like Structure. *Phys. Rev. B* **2007**, *76* (12), 125421.
(45) Kaplan-Ashiri, I.; Cohen, S. R.; Gartsman, K.; Rosentsveig, R.; Seifert, G.; Tenne, R. Mechanical Behavior of Individual Ws2 Nanotubes. *J. Mater. Res.* **2004**, *19* (2), 454−459.
(46) Kohler, T.; Frauenheim, T.; Hajnal, Z.; Seifert, G. Tubular Structures of Gas. *Phys. Rev. B* **2004**, *69* (19), 193403.